Available online at www.eccomasproceedia.org
Eccomas Proceedia SMART (2023) 560-571

ECCOMAS
Proceedia

X ECCOMAS Thematic Conference on Smart Structures and Materials
SMART 2023
D.A. Saravanos, A. Benjeddou, N. Chrysochoidis and T. Theodosiou (Eds)

ACTIVE STIFFNESS TAILORING OF HYBRID SMP-CARBON EPOXY BI-STABLE TAPE SPRINGS

Aghna Mukherjee*, Severin Huber*, Paolo Ermanni*

*Laboratory of Composite Materials and Adaptive Structures (CMASLab)
Department of Mechanical and Process Engineering
ETH Zurich, Leonhardstrasse 21, 8092, Zürich
e-mail: amukherj@ethz.ch, web page: http://https://structures.ethz.ch/
.

Key words: Bistable laminates, Multiphysics Problems, Shape Memory Polymers, Finite Element Method

Abstract. In the past, metal, polymer, and composite-based mono-stable and bi-stable tape springs have been used in space applications as deployable hinges and booms. At the CMASLab, we are exploring ways to expand their utility by incorporating them as design components in reconfigurable structures. For bi-stable tape springs to be suitable for structural purposes, they need to exhibit adequate stiffness in both stable states. However, the stiffness, particularly in the curved state, is often insufficient for many structural applications. In this study, we develop a new hybrid SMP-carbon epoxy bi-stable tape spring by co-curing carbon-epoxy and SMP layers in an autoclave. Initial analysis and experiments demonstrate that the resulting hybrid composite exhibits significantly enhanced stiffness in both stable configurations. Furthermore, the bistability can be toggled, and the stiffness can be extensively customized by applying an external heat stimulus to regulate the temperature of the SMP layer. When the SMPs are heated beyond their glass transition temperature, their elastic modulus decreases by a factor of ten. This temperature-dependent change in elastic modulus facilitates both stiffness customization and bistability activation and deactivation. To better comprehend the design possibilities of this novel concept, a numerical model is created in ABAQUS^{TM} to simulate the snap-through and the impact of temperature on the system's bistability and stiffness. The design space analysis reveals that the hybrid structure's performance is highly sensitive to the layup and the relative thickness of the SMP and carbon-epoxy layers. The developed concepts have the potential to be employed in the reconfiguration of lightweight space structures with minimal energy expenditure.

1 INTRODUCTION

Bistable tape springs are thin-walled shell structures with one or two stable configurations depending on the geometry and layup [1, 2]. Their unique behavior has inspired several structural applications involving shape adaptation, especially in developing deployable space structures

Peer-review under responsibility of the organizing committee of SMART 2023.
doi: 10.7712/150123.9810.445415

[3, 4]. All adaptive structures must fulfill the contradictory requirements of stiffness to carry loads and the capability of low-energy shape change while complying with strict mass and volume constraints [5, 6, 7]. In most deployment concepts, the tape springs are held in a deformed configuration in a stressed state using a hold-down and release mechanism. On deployment (activation of the release mechanism), the stored potential energy enables the tape springs to unfold and reach the stiff deployed state. It is seen in the literature that there is a substantial difference in the stiffnesses of the straight (stiff state) and the folded configuration (lower stiffness state) [8]. Since in deployment applications, the tape spring spends most of the operation time in the stiff configuration, the lower stiffness of the coiled configuration is acceptable.

While most applications using tape springs have focused on deployment, CMASLab is developing a new class of reconfigurable hinges in collaboration with Clearspace. Using bistable tape springs for reconfiguration requires a balance between the stiffness (the requirements depend on the operation) and the force required for the reversible snapping. And the stiffnesses of both stable configurations become relevant design parameters. The stiffness of these structures can be increased in either configuration by increasing thickness. However, this adds to the actuation complexities and increases the maximum stresses generated during the snapthrough. New design strategies are required to extend the utility of tape springs to applications that require more functionality than one-time deployments, like reconfiguration of solar panels or sensing devices like antennas [9, 10].

Recently, shape memory polymers (SMPs) have received much attention from the research community for their potential in designing adaptive structures [11]. Shape memory polymers (SMPs) can change shape in response to a stimulus such as heat, light, or environmental change [12]. While several challenges of using shape memory polymers have been identified in the literature [13, 14], their unique property of changing stiffness by one or two orders of magnitude in response to heat makes them very promising in designing adaptive structures [15, 16].

Various examples in the literature demonstrate the use of Shape Memory Polymers (SMPs) for creating variable stiffness structures [17], but these structures tend to have limited load-bearing capacity. This paper introduces an innovative SMP-Carbon Fiber Reinforced Polymer (CFRP) hybrid bistable composite that merges CFRP and SMP layers into a hybrid structure. The SMP layers allow for stiffness adjustment through an external heat stimulus, while the CFRP laminate offers the essential load-carrying abilities. When the temperature of the SMP-CFRP hybrid tape spring exceeds the glass transition temperature of the SMP, T_g, the SMP layer's stiffness decreases significantly, leading to a complete alteration in the system's structural behavior. The SMP exhibits considerable stiffness at temperatures below T_g, resulting in a highly stiff structure. Elevating the hybrid tape spring's temperature above T_g diminishes the stiffness, facilitating the snapthrough transition to another state. After snapping, the structure cools down and achieves a rigid second state. This innovative architecture significantly enhances the stiffness of the structure compared to the original tape spring in both configurations, while maintaining relatively low snapthrough loads and generated stresses during the snapping process.

2 HYBRID SMP-CFRP CONCEPT

Tape springs have two stable configurations. Applying a load/moment, it is possible to go between the stable states; however, there is a trade-off between the stiffness and the force

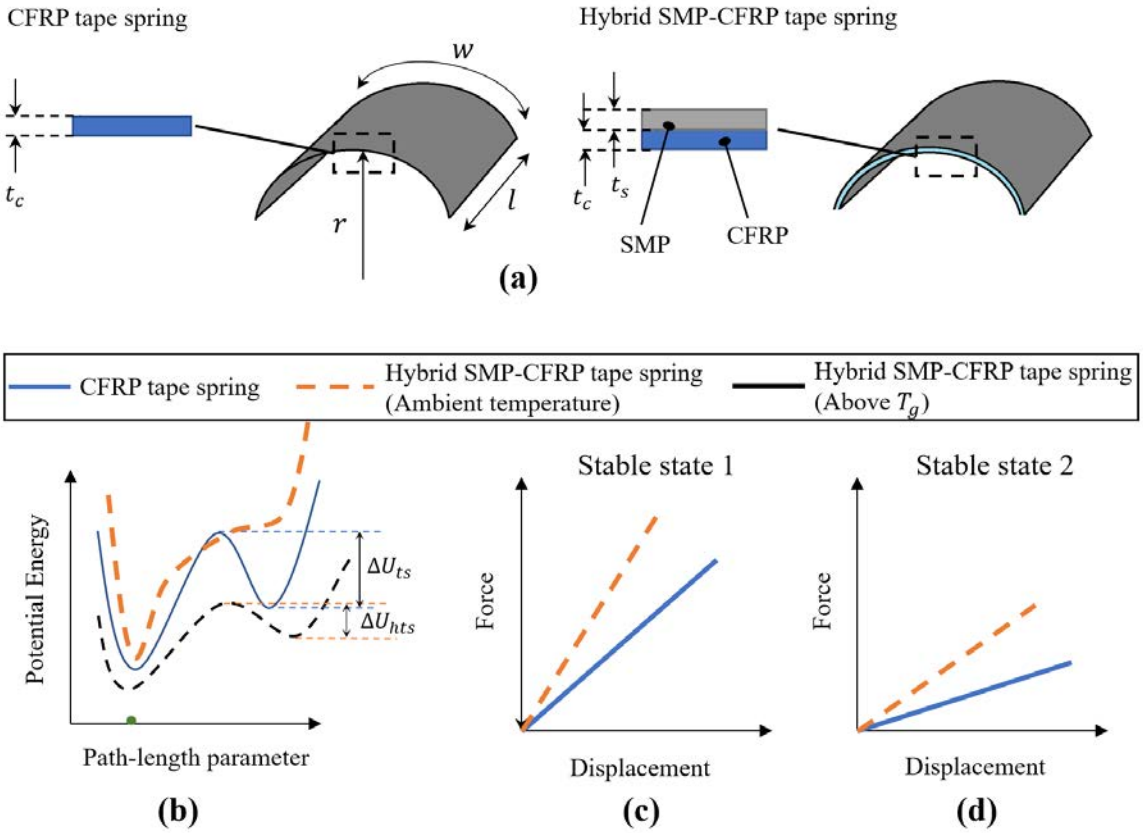

Figure 1: (a) The layup and the geometric parameters of the hybrid SMP-CFRP concept. (b) Qualitative comparison of potential energy functions for CFRP tape spring and the hybrid SMP-CFRP concept. The potential energy of the SMP-CFRP concept is plotted at temperatures above and below T_g. (c) and (d) The load-displacement diagram considering small deformations starting from the equilibrium states 1 and 2, respectively.

required for reconfiguration. Moreover, the curved configuration has much lower stiffness in bending than the straight stiff configuration. The new architecture proposed in this manuscript, shown in Fig. 1(a), combines the CFRP tape springs with an additional layer of SMP. The SMP layer provides active stiffness tailoring under an external stimulus of heat. At room temperature, the SMPs are below their glass transition temperature T_g, and on heating above T_g, the stiffness of the SMP layer reduces substantially.

Depending on the relative thickness of the SMP compared to the CFRP layer t_s/t_c and the layup, the behavior of the SMP-CFRP hybrid structure can be quite different. The baseline hybrid laminate in this manuscript is selected as $[\text{SMP}/(-45/45)_4]_T$, where the thickness of the SMP layer is t_s. A representative plot showing the potential energy of a CFRP tape spring and the hybrid structure at temperatures above and below T_g is shown in Fig. 1(b). The baseline hybrid structure is monostable at room temperature. However, it is possible to access the second stable state by increasing the temperature of the SMP above T_g and snapping the laminate.

The addition of the SMP layer increases the structure's stiffness in both stable configurations, as shown in Fig. 1(c) and (d). Additionally, it is also seen that the snapthrough load required to snap the laminates between the two stable states at an elevated temperature is much lower than an equivalent stiffness CFRP tape spring (see Fig. 1(b)).

2.1 Materials and Manufacturing

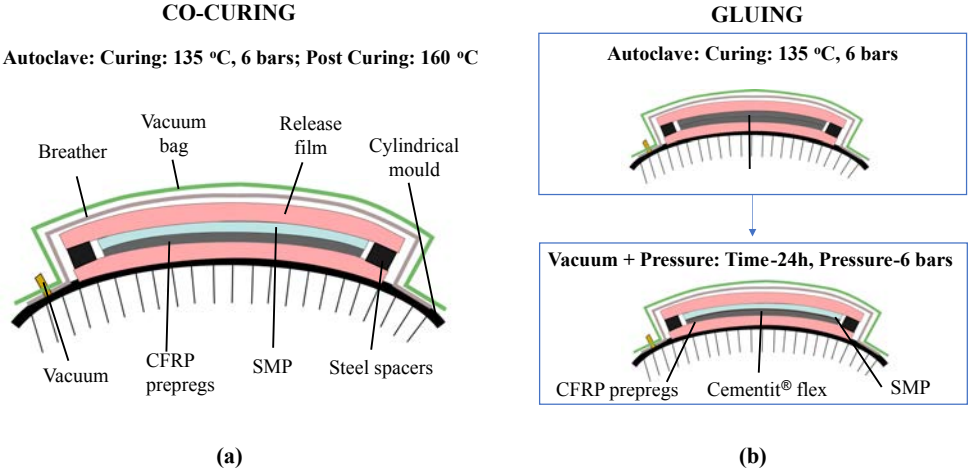

Figure 2: Schematic for the fabrication process: (a) co-curing and (b) gluing.

The composite tape spring structures are manufactured using T700 carbon fibers and Thinpreg 513 prepregs procured from NTPT [18]. While the modified architecture is made using two SMPs, PETG, and a Vero material RGD8520 [19]. The Vero materials can be 3D printed using the PolyJet process, making more complex constructions possible. The material properties of the CFRP and the SMPs are given in Tables 1 and 2, respectively.

The hybrid composites are manufactured using two methods:

1. *Co-curing*: In this method, the CFRP prepregs and SMP layers are co-cured together on a cylindrical mold in an autoclave using the manufacturer-specified curing cycle, followed by a two-hour post-curing cycle at 160 °C. [18]. The schematic for the fabrication is shown in Fig 2(a).

2. *Gluing*: The CFRP part is manufactured separately in an autoclave using the standard autoclave manufacturing process [20, 21]. Subsequently, the CFRP part is glued to the SMP layer using flexible glue Cementit^R Flex. This glue can resist temperatures between -40 °C to 110 °C. Cementit^R Flex requires an initial curing for an hour followed by a secondary curing of 24 hours, according to the manufacturer's recommendations. The process schematic is shown in Fig 2(b).

All the tape springs manufactured have the same dimensions, $l = 50$ mm, $w = 50$ mm, and $r = 25$ mm. Two layups have been manufactured and tested, $[\text{SMP}/(-45/45)_4]_T$ and $[(-45/45)_2/\text{SMP}/(-45/45)_2]_T$.

Table 1: Material properties of the carbon-epoxy unidirectional prepreg (T700/TP513)

Material	E_1[GPa]	E_2[GPa]	ν_{12}	G_{12}[GPa]	ν_f	t [mm]
T700/TP513	132	8	0.253	4.05	57	0.034

Table 2: Material properties of PETG and RGD8520 [18, 19]

Material	E [MPa]	ρ [g/cm^3]	T$_m$[°C]	T$_g$[°C]	T$_D$[°C]
PETG	1800	1.27	80	180	400
RGD8520	2100	-	55	320	250

2.2 FEM simulation

The hybrid SMP-CFRP laminates are modeled in ABAQUS^{TM} considering geometric nonlinearities using quadrilateral shell elements (S4R). In the FE model, the properties of the CFRP are assumed to be linear elastic. The SMP's mechanical properties vary broadly with temperature. Hence temperature dependent material properties are used for the simulation. The SMPs have a very low recovery force. A small stress of $\sigma < 4$ MPa can lead to a complete loss of recovery [22]. The stresses generated in the laminate during the snapthrough are substantially higher than 4 MPa. Hence, to capture the permanent deformation, the model uses a simplifying assumption of plastic deformation, ignoring the shape recovery. Moreover, it is assumed that the yield stress of SMPs ($\sigma_{y_{\text{SMP}}}$) reduces substantially beyond the glass transition temperature (T_g),

Two models are created using ABAQUS^{TM}. The first model simulates the snapthrough of hybrid tape springs at ambient temperature and consists of three steps: (a) *Frequency step*: eigenvalues of the stable state are determined through natural frequency analysis. (b) *Fold step*: snapthrough is simulated with a dynamic implicit procedure, accompanied by a release step. (c) *Frequency step*: natural frequencies are assessed for the second stable configuration. In this paper, the room temperature snapthrough is termed "*cold fold*."

The second model deals with snapthrough at a higher temperature and includes six steps: (a) *Frequency step*: natural frequency is calculated for the initial configuration. (b) *Heating step*: hybrid laminate is heated beyond its glass transition temperature (T_g). (c) *Fold step*: forces are applied to the laminate, causing it to snap into the second equilibrium configuration using a dynamic implicit quasi-static procedure. (d) *Release step*: loads are removed, allowing the laminate to relax to the nearest stable configuration with the aid of a static STABILIZE procedure. (e) *Cooling step*: temperature is lowered to ambient conditions. (f) *Frequency step*: natural frequency analysis is performed again to determine the natural frequency of the second stable configuration. This simulation is termed as "*hot fold*."

In this paper, the natural frequency is utilized to measure the stiffness of hybrid laminates in two states. The lowest stiffness is represented by the first eigenfrequency, and the corresponding eigenvector indicates the direction of minimal stiffness. In the finite element (FE) models, if the eigenvalues of the initial configuration and the stable state acquired after snapthrough are identical, it suggests that the structure possesses only a single stable equilibrium configuration. The two FE analyses are illustrated in Figs. 3(top) and 3(bottom).

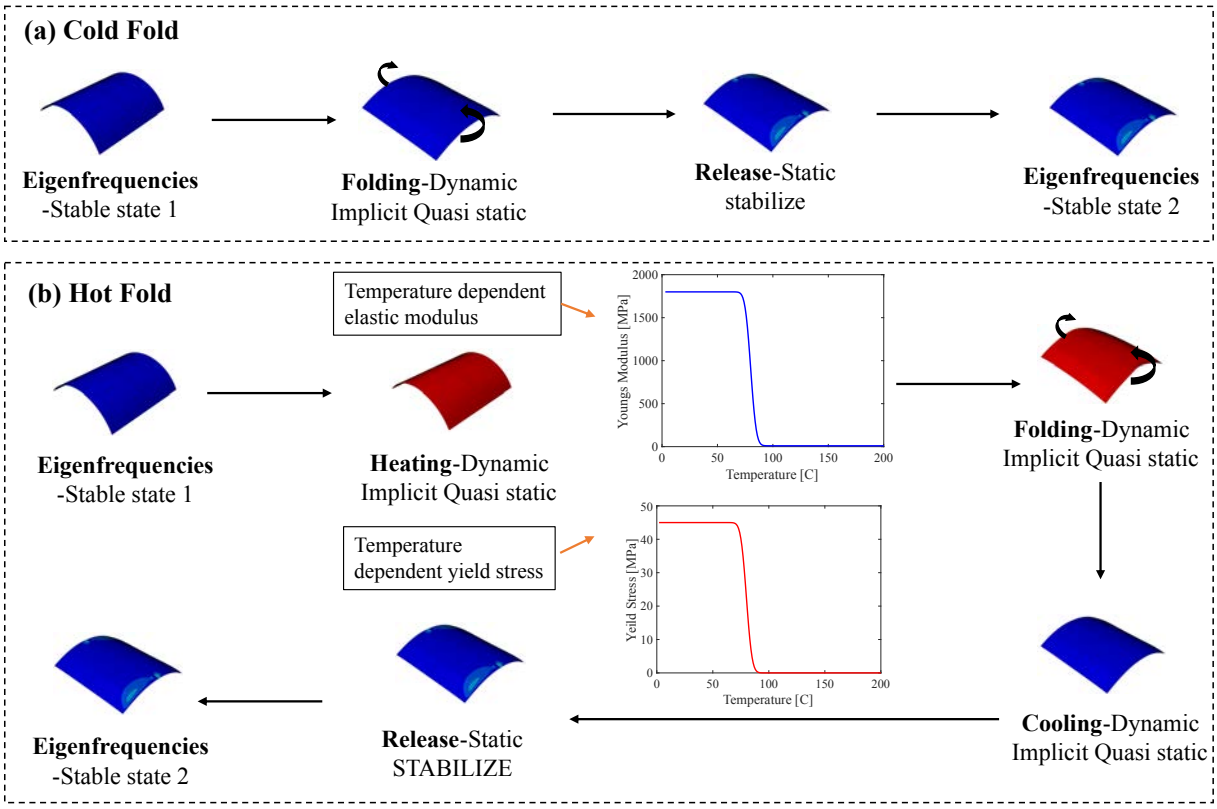

Figure 3: Flowchart showing the FE analysis steps for (top) the "*cold fold*" simulation and (c) the "*hot fold*" simulation in ABAQUS^{TM}.

3 HYBRID TAPE SPRING PERFORMANCE

3.1 Manufacturing methods

As outlined in Section 2.1, two methods are employed to manufacture the SMP-CFRP hybrid composites: co-curing and gluing. In order to assess the quality of the produced samples, a four-stage experiment is devised: First, bistability is examined at room temperature (i.e., $T < T_g$). Next, the samples are heated in an oven. Subsequently, bistability is re-evaluated at the increased temperature (i.e., $T > T_g$). Lastly, the samples are cooled below T_g while in their second stable state.

The baseline sample, denoted as $[\text{SMP}/(-45/45)_4]T$, with an SMP layer thickness of $t_s = 0.3$ mm, does not exhibit bistability at room temperature. However, as the temperature increases, the hybrid sample transitions into a bistable state. When cooled, the hybrid laminate maintains its second equilibrium configuration. To assess manufacturing quality, the heating-snapthrough-cooling cycle is repeated 25 times. Although both methods yield structures with the anticipated mechanical properties, initial findings suggest that the co-curing process is more effective. In glued samples, air pockets are present. Figure 4(a) displays two RGD8520-CFRP laminate samples produced by gluing; the top sample utilizes Cementit Flex, while the bottom sample employs Loctite 454^{TM} glue. Enclosed air pockets can be observed between the glued interfaces,

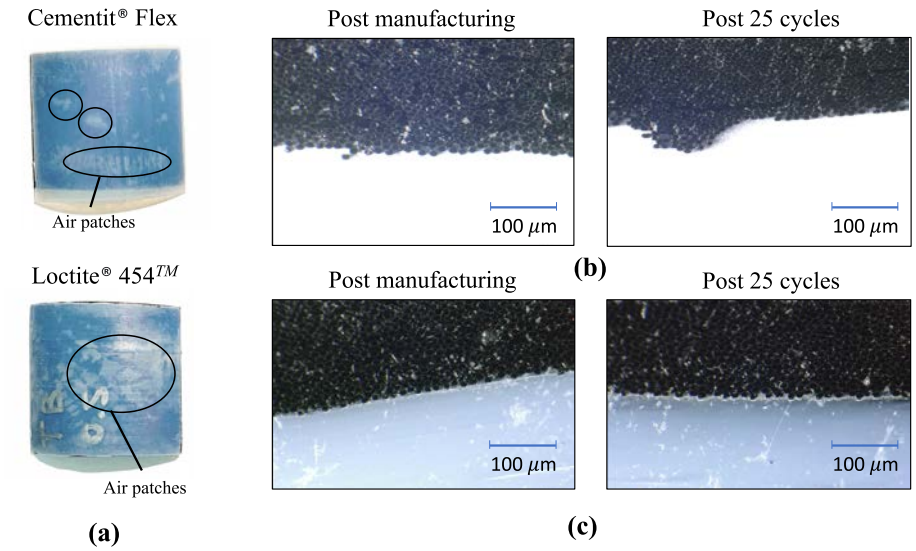

Figure 4: (a) SMP-CFRP glued samples. (b) Micrographs of PETG-CFRP and RGD8520 samples post-manufacturing and after 25 thermo-mechanical actuation cycles.

and these pockets tend to increase with successive thermomechanical cycles. However, since PETG is opaque, a similar visual inspection cannot be conducted for the PETG-CFRP glued sample.

Figures 4(b) and (c) show the micrographs of co-cured samples of PETG-CFRP and RGD8520-CFRP hybrid laminates. A clear distinction can be seen between the SMP and the CFRP layer. It is seen that voids are present in the CFRP layer but not at the interface of CFRP and SMP. Also, it can be observed that the micrographs of the pristine samples and the samples that have undergone 25 heating-snapthrough-cooling cycles are qualitatively almost the same.

3.2 Stiffness tailoring and snapthrough

Figure 5(a) shows the stiffness of the two stable states for the baseline $[\text{SMP}/(-45/45)_4]_T$, $\text{SMP} \in [\text{PETG}, \text{RGD8520}]$ samples compared to a CFRP laminate with the layup $[(-45/45)_4]_T$. It's worth noting that at room temperature, the two SMP samples are monostable. Nonetheless, when subjected to a heating-folding-cooling cycle, the laminate transitions to the second stable configuration. The laminate doesn't revert to the initial equilibrium state upon cooling since shape recovery doesn't take place. For shape recovery to occur, the laminate stresses need to be less than or equal to 4 MPa.

The stiffness of the hybrid laminate, compared to the CFRP laminate with the same layup, is significantly higher (measured in terms of the first natural frequency). The PETG-CFRP hybrid composite experiences a 24.338 % increase in stiffness for the first state, while the RGD8520-CFRP hybrid composite exhibits a 29.45% rise. In the second equilibrium state, the increase is even more pronounced. The PETG-CFRP composite demonstrates a 60.93% increase in stiffness, and the RGD8520-CFRP composite displays a 68.70% improvement.

Fig 5(b) shows the load-displacement diagrams for the baseline $[\text{PETG}/(-45/45)_4]_T$ laminate, a $[\text{RGD8520}/(-45/45)_4]_T$ laminate and a laminate without the SMP layer $[(-45/45)_4]_T$.

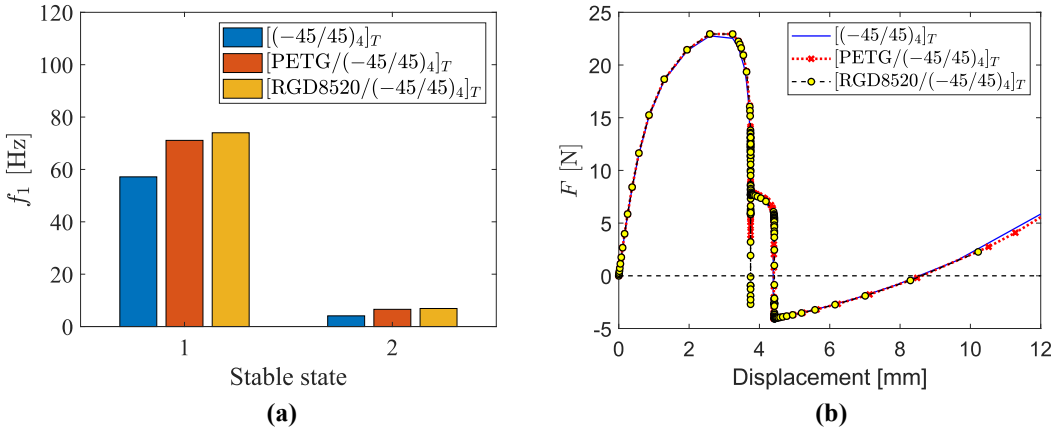

Figure 5: (a) The first eigenfrequency of the $[(-45/45)_4]_T$, $[\text{PETG}/(-45/45)_4]_T$, and $[\text{RGD8520}/(-45/45)_4]_T$ samples in the original equilibrium state (straight stiff state) and the second equilibrium configuration (coiled flexible state) obtained using FE analysis in ABAQUS^{TM}. (b) The force-displacement diagram of the snapthrough for $[(-45/45)_4]_T$, $[\text{PETG}/(-45/45)_4]_T$ and $[\text{RGD8520}/(-45/45)_4]_T$ laminates obtained using ABAQUS^{TM}.

The snapthrough simulation for the $[(-45/45)_4]_T$ CFRP sample is done at room temperature. However, the *hot fold* simulation is used for the hybrid samples, as the laminate is not bistable at room temperature. It can be observed that while the stiffness of the hybrid sample increases substantially, the snapthrough loads of the two laminates are almost the same.

3.3 An alternate sandwich architecture for the hybrid tape springs

In this subsection, an alternate architecture is introduced, where the SMP layer is sandwiched between the CFRP layers as shown in Fig. 6(a). It is interesting to note that compared to the baseline laminate, the new architecture $[(-45/45)_2/\text{SMP}/(-45/45)_2]_T$ with $t_s = 0.3$ mm is bi-stable at both the room temperature and above T_g. Figure 6(b) shows the first natural frequency at the two stable states as a function of the SMP layer thickness for the new architecture. The laminate is found to be bi-stable till a critical thickness, using both the *cold fold* and *hot fold* simulations. Beyond the critical length, the laminate loses bistability at both ambiance and at a temperature higher than T_g.

3.3.1 An interesting behavior!

The loss of bistability with the increase in thickness is the expected behavior. However, an interesting phenomenon occurs when the SMP thickness, t_s ranges between $(0.66, 0.7)$ mm, where the hybrid laminate exhibits bistability at room temperature, while it is monostable at temperatures higher than T_g. Figure 6(c) shows two simulations in ABAQUS^{TM}. In the first simulation, the snapthrough is done at a temperature above T_g. After releasing the actuation force, the laminate returns to the first stable configuration. In the second simulation, the folding (snapthrough) is done at room temperature. It can be seen in the schematic that the laminate transitions to the second state. Additionally, a heating step simulation following snapping

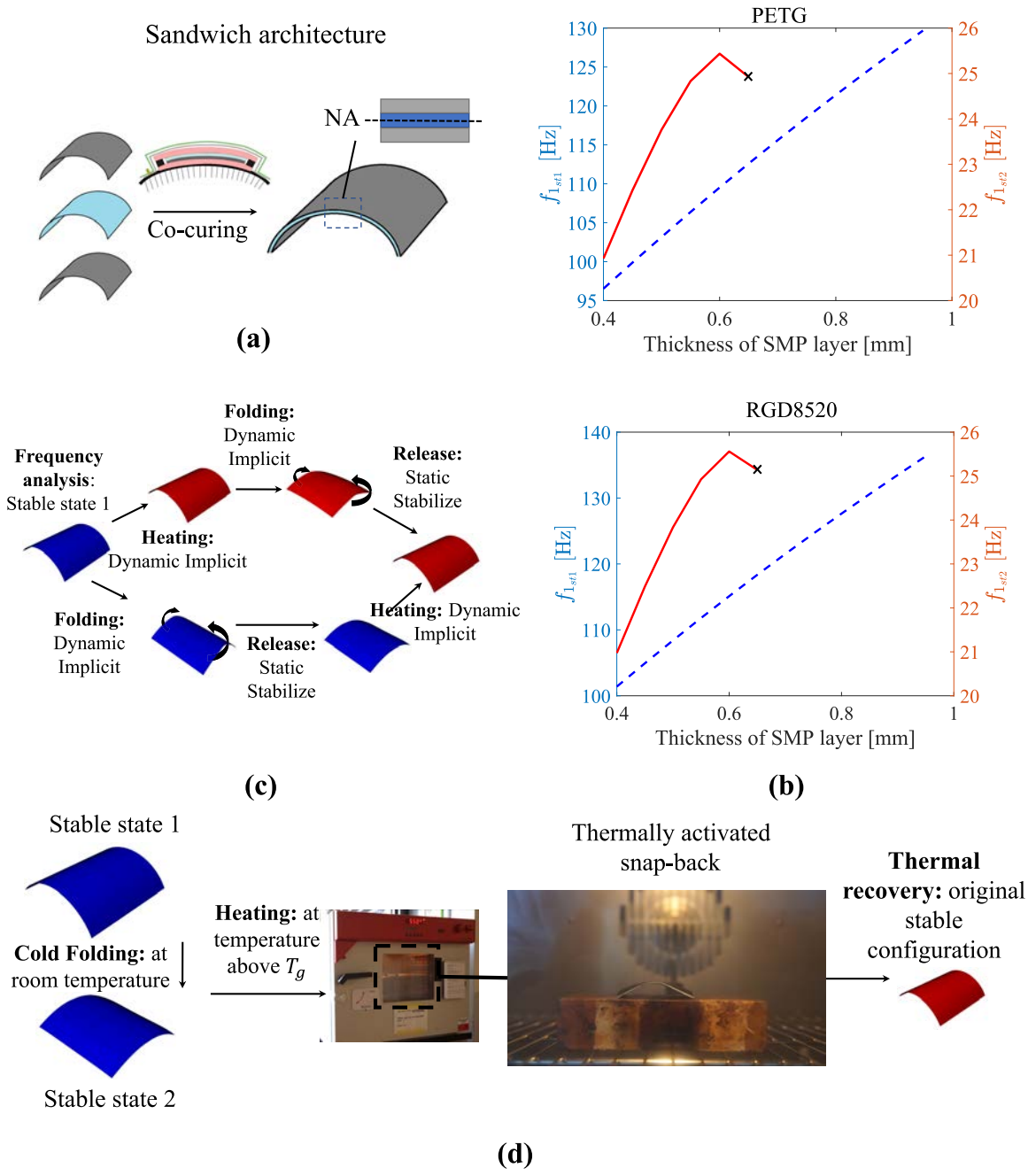

Figure 6: (a) The schematic of the alternate sandwich architecture for the SMP-CFRP hybrid composites. (b) The first natural frequency f_1 plotted as a function of SMP thickness for PETG-CFRP (top) and RGD8520-CFRP (bottom) laminates. (c) Schematic of the *Cold fold* and *hot fold* numerical simulations conducted for the new architecture in the SMP thickness range of $t_s \in (0.65, 0.7)$ mm. (d) Experimental schema for replicating the strange behavior and showing the possibility of achieving temperature activated snapping.

causes the laminate to revert to the initial stable configuration. This demonstrates that, within a narrow thickness range, the sandwich architecture can achieve snapthrough without external force, relying solely on temperature stimulus. The stiffnesses of the two states obtained using the *cold fold* and *hot fold* simulations in ABAQUS^{TM} are summarized in Table 3. The absence of the first natural frequency of state 2 indicates that a successful snapthrough was not achieved.

The thermally activated snapthrough was experimentally validated. A number of $[(-45/45)_2/\text{PETG}/(-45/45)_2]_T$ samples with thicknesses in the range $t_s \in (0.3, 0.7)$ mm were fabricated for stability testing. Figure 6(e) outlines the steps employed to achieve thermal snapping. First, the laminate is *cold-folded* at room temperature. The samples that transitioned to the second state were then heated in a Binder oven. It was observed that the samples with thicknesses between 0.3 and 0.4 mm successfully transitioned to the second stable state; however, the original equilibrium configuration could not be recovered upon heating. The sample with a PETG thickness of 0.5 mm transitioned to the second state when heated, which is lower than the thickness predicted by the FE model. Thicker samples were monostable, regardless of the snapping temperature.

Table 3: The stability behavior for SMP-CFRP hybrid composites in this narrow thickness range of $\in (0.65, 0.7)$ mm.

		PETG		**RGD8520**	
SMP thickness [mm]	Folding temperature [^{0}C]	f_1 (State 1) [Hz]	f_1 (State 2) [Hz]	f_1 (State 1) [Hz]	f_1 (State 2) [Hz]
0.67	$T \leq T_G$	113.2	24.461	118.99	24.736
	$T \geq T_G$	113.2		118.99	
0.68	$T \leq T_G$	113.81	23.737	119.63	24.126
	$T \geq T_G$	113.81		119.63	
0.69	$T \leq T_G$	114.41	22.389	120.26	23.03
	$T \geq T_G$	114.41		120.26	
0.70	$T \leq T_G$	115	17.606	120.89	20.379
	$T \geq T_G$	115		120.89	

4 CONCLUSION AND OUTLOOK

This manuscript introduces a novel hybrid SMP-CFRP composite laminate. The SMP layer in the hybrid composite enables active stiffness tailoring and a complete change in the system's stability behavior using an external temperature stimulus. This unique behavior is achieved by leveraging the significant variation of the stiffness modulus of SMPs with temperature. Preliminary analysis and experiments demonstrate that the stiffness of the two stable configurations can be significantly increased using this concept while maintaining snapthrough loads comparable to the base CFRP laminate. Furthermore, bistability can be switched on and off as needed. It is evident that the hybrid composite's properties are highly sensitive to the relative thickness of the SMP and CFRP layers. Careful tuning of the hybrid composite parameters can lead to thermally activated snapthrough. This concept offers a way to enhance the load-bearing capacity of reconfigurable structures without impacting compliance.

The promising behavior exhibited in this initial study holds great potential for developing

adaptive structures. However, the manufacturing techniques employed in the paper need improvement. A deeper understanding of sensitivities to different processing conditions is required. Additionally, the FE model developed for this study makes some simplifying assumptions that overlook the shape recovery behavior of SMPs. While this assumption is valid for relatively thicker laminates, the effect of shape recovery becomes relevant as thickness decreases (which might apply, for instance, to micro-robotics applications). Lastly, numerous challenges associated with using SMPs in harsh environments still demand further investigation.

5 ACKNOWLEDGEMENT

The authors express their sincere gratitude to the Swiss Innovation Agency - Innosuisse for funding the project, titled "Inspection Arm for On-Orbit Servicing" (Grant no.: 52266.1 IP-ENG). The authors also extend their appreciation to Ms. Alina Arranhado for her initial contributions to manufacturing and testing the hybrid samples.

References

[1] E. Kebadze, S. Guest, and S. Pellegrino, "Bistable prestressed shell structures," *International Journal of Solids and Structures*, vol. 41, no. 11-12, pp. 2801–2820, 2004.

[2] S. Guest and S. Pellegrino, "Analytical models for bistable cylindrical shells," *Proceedings of the Royal Society A: Mathematical, Physical and Engineering Sciences*, vol. 462, no. 2067, pp. 839–854, 2006.

[3] J. Costantine, Y. Tawk, C. G. Christodoulou, J. Banik, and S. Lane, "Cubesat deployable antenna using bistable composite tape-springs," *IEEE Antennas and Wireless Propagation Letters*, vol. 11, pp. 285–288, 2012.

[4] H. Mao, P. L. Ganga, M. Ghiozzi, N. Ivchenko, and G. Tibert, "Deployment of bistable self-deployable tape spring booms using a gravity offloading system," *Journal of Aerospace Engineering*, vol. 30, no. 4, p. 04017007, 2017.

[5] S. A. Emam and D. J. Inman, "A review on bistable composite laminates for morphing and energy harvesting," *Applied Mechanics Reviews*, vol. 67, no. 6, 2015.

[6] I. K. Kuder, A. F. Arrieta, W. E. Raither, and P. Ermanni, "Variable stiffness material and structural concepts for morphing applications," *Progress in Aerospace Sciences*, vol. 63, pp. 33–55, 2013.

[7] A. Mukherjee, D. Kumar, S. F. Ali, and A. Arockiarajan, "Design and conception of a trailing edge morphing wing concept with bistable composite skin," in *Active and Passive Smart Structures and Integrated Systems XIV*, vol. 11376. SPIE, 2020, pp. 497–506.

[8] E. Gdoutos, A. Truong, A. Pedivellano, F. Royer, and S. Pellegrino, "Ultralight deployable space structure prototype," in *AIAA Scitech 2020 Forum*, 2020, p. 0692.

[9] W. R. Doggett, J. T. Dorsey, T. C. Jones, and B. King, "Development of a tendon-actuated lightweight in-space manipulator (talisman)," in *The 42nd Aerospace Mechanism Symposium*, 2014.

[10] M. Sakovsky and P. Ermanni, "Structurally reconfigurable antennas for spacecraft," in *AIAA Scitech 2021 Forum*, 2021, p. 1495.

[11] A. J. McClung, G. P. Tandon, and J. W. Baur, "Strain rate-and temperature-dependent tensile properties of an epoxy-based, thermosetting, shape memory polymer (veriflex-e)," *Mechanics of Time-Dependent Materials*, vol. 16, pp. 205–221, 2012.

[12] Y. Liu, H. Du, L. Liu, and J. Leng, "Shape memory polymers and their composites in aerospace applications: a review," *Smart Materials and Structures*, vol. 23, no. 2, p. 023001, 2014.

[13] S. Y. Park, H. S. Choi, W. J. Choi, and H. Kwon, "Effect of vacuum thermal cyclic exposures on unidirectional carbon fiber/epoxy composites for low earth orbit space applications," *Composites Part B: Engineering*, vol. 43, no. 2, pp. 726–738, 2012.

[14] J. Chen, N. Ding, Z. Li, and W. Wang, "Organic polymer materials in the space environment," *Progress in Aerospace Sciences*, vol. 83, pp. 37–56, 2016.

[15] L. Santo, F. Quadrini, and D. Bellisario, "Shape memory composite antennas for space applications," in *IOP Conference Series: Materials Science and Engineering*, vol. 161, no. 1. IOP Publishing, 2016, p. 012066.

[16] J.-H. Roh, H.-J. Kim, and J.-S. Bae, "Shape memory polymer composites with woven fabric reinforcement for self-deployable booms," *Journal of intelligent material systems and structures*, vol. 25, no. 18, pp. 2256–2266, 2014.

[17] H. Niknam, A. Akbarzadeh, D. Therriault, and S. Bodkhe, "Tunable thermally bistable multi-material structure," *Applied Materials Today*, vol. 28, p. 101529, 2022.

[18] *NTPT Thinpreg 513 Data Sheet*, North Thin Ply Technologies, 2017, https://www.thinplytechnology.com/assets/mesimages/NTPT-DS-ThinPreg-513-April2017-v3.pdf.

[19] *Digital Materials Data Sheet*, Stratasys, 2017, https://www.stratasys.com/siteassets/materials/materials-catalog/polyjet-materials/digital-abs-plus/mss_pj_digitalmaterialsdatasheet_0617a.pdf.

[20] A. Mukherjee, M. I. Friswell, S. F. Ali, and A. Arockiarajan, "Modeling and design of a class of hybrid bistable symmetric laminates with cantilever boundary configuration," *Composite Structures*, vol. 239, p. 112019, 2020.

[21] A. Mukherjee, S. F. Ali, and A. Arockiarajan, "Hybrid bistable composite laminates for structural assemblies: A numerical and experimental study," *Composite Structures*, vol. 260, p. 113467, 2021.

[22] F. Ji, Y. Zhu, J. Hu, Y. Liu, L.-Y. Yeung, and G. Ye, "Smart polymer fibers with shape memory effect," *Smart materials and Structures*, vol. 15, no. 6, p. 1547, 2006.